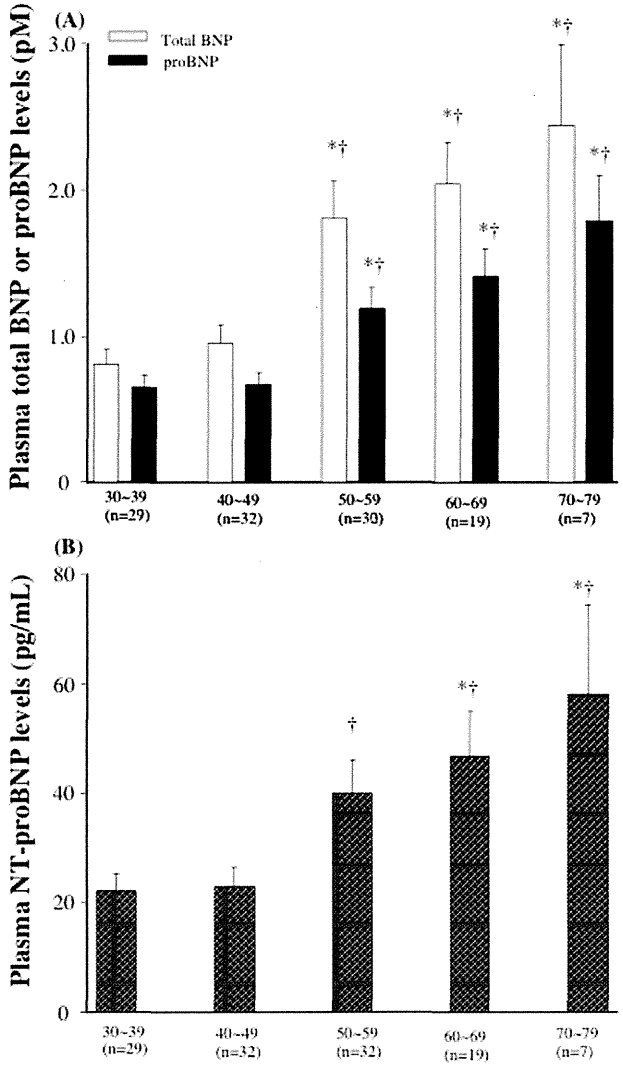

Figure 4. Plasma Levels of total BNP, proBNP, and NT-proBNP in different age groups. Bar graph showing the total BNP, proBNP (A) and NT-proBNP levels (B). Values are means ± SE., *P<0.05 vs total BNP, proBNP, and NT-proBNP in 30~39, †P<0.05 vs total BNP, proBNP, and NT-proBNP in 40~49.
doi:10.1371/journal.pone.0053233.g004

When we then assessed the intra- and inter-assay precision using plasma spiked with glycosylated proBNP or BNP, we found that the intra-assay CV ranged from 5.2%–8.0% in proBNP assay and from 7.0%–8.4% in total BNP assay, while inter-assay CV ranged from 5.3–7.4% in proBNP assay and from 1.9%–9.5% in total BNP assay, respectively (Table 3, 4).

Specificity and sensitivity

We next examined the cross-reactivity between proBNP and BNP. As shown in Table 5, the presence of BNP did not affect the values measured with the proBNP assay system. Moreover, the values measured with the total BNP assay system were the sum of the BNP and proBNP even at different compositions of these two peptides. Thus, the total BNP assay recognized both BNP and proBNP with the same efficiency and sensitivity. Likewise, the proBNP and total BNP assay systems recognized proBNP with the same efficiency and sensitivity.

Gel-filtration chromatography before and after deglycosylation procedure

Figure 3-A shows two immunoreactive BNP peaks detected using the total BNP assay with HPLC fractions. The first peak appeared in fractions 52–55 and the second peak in fractions 72–75. With the same sample, one immunoreactive BNP peak was detected by the proBNP assay (Figure 3-B); the position of that peak was completely consistent with the proBNP peak obtained with the total BNP assay. When subjected to gel filtration HPLC, recombinant proBNP, glycosylated proBNP and BNP were eluted mainly in fractions 53, 56 and 74, respectively. Treating the same plasma sample with an enzyme cocktail catalyzing deglycosylation shifted the first peak to fraction 54–56, which is consistent with the proBNP peak. From these results, we conclude that total BNP assay evaluates the sum of the glycosylated proBNP plus BNP, while proBNP assay detects glycosylated proBNP. The proBNP was not detected in a significant level with either assay system.

Plasma concentrations of proBNP, total BNP, and NT-proBNP in healthy subjects and heart failure patients

Plasma total BNP, proBNP and NT-proBNP levels in different age groups were shown in Figure 4-A, B. Plasma total BNP, proBNP and NT-proBNP levels appeared to increase according to the age. The older age groups (more than 50) had higher total BNP, proBNP and NT-proBNP levels than younger age groups (less than 50); however, there were no statistical differences in NT-proBNP between 30~39 and 50~59. In addition, there were significant positive relationships between plasma total BNP ($r=0.467$, $p<0.001$), proBNP ($r=0.491$, $p<0.001$) and NT-proBNP ($r=0.376$, $p<0.001$) levels and age (Figure 5-A, B, C).

The mean total BNP and proBNP in plasma from 116 healthy subjects were 1.4±1.2 pM and 1.0±0.7 pM, respectively (Figure 6-A). Female had higher total BNP than male (total BNP: 1.7±1.3 vs 1.1±1.1, $P<0.05$; proBNP: 1.1±0.8 vs 0.8±0.6 pM, $P=0.11$) (Figure 6-C). proBNP/total BNP ratio was lower in female than that in male. NT-proBNP was also higher in female than those in male (Figure 6-E). The total BNP and proBNP levels were markedly elevated in heart failure patients, and the magnitude of the increase reflected the severity of the patients' condition as observed in NT-proBNP (Figure 6-A, B).

Discussion

Plasma levels of the cardiac hormone BNP increase in proportion to the severity of heart failure. Indeed, plasma BNP levels are used as a biomarker of heart failure, and the guidelines in many countries recommend that BNP be used as a diagnostic indicator of acute and chronic heart failure [1–3]. The stimuli that increase cardiac BNP production include pressure overload, volume overload and ischemia, as well as various cytokines and neurohumoral factors [15]. In response to these stimuli, BNP mRNA expression is rapidly upregulated. Following translation of the protein, the signal peptide is removed to produce proBNP, which is then cleaved into BNP and the NT-proBNP fragment during secretion [15]. It is noteworthy that BNP and proBNP could not be distinguished from one another in earlier BNP assay systems because the anti-BNP antibodies cross-reacted with proBNP. We therefore endeavored to develop a new assay system that would enable separate measurement of BNP and proBNP. Recent studies have shown that levels of uncleaved proBNP are increased in heart failure to a greater degree than BNP [5–7,16]. Using a combination of gel filtration and an immunoenzyme fluorescent assay for BNP, we previously found that proBNP levels are increased in heart failure and that the proBNP/total BNP

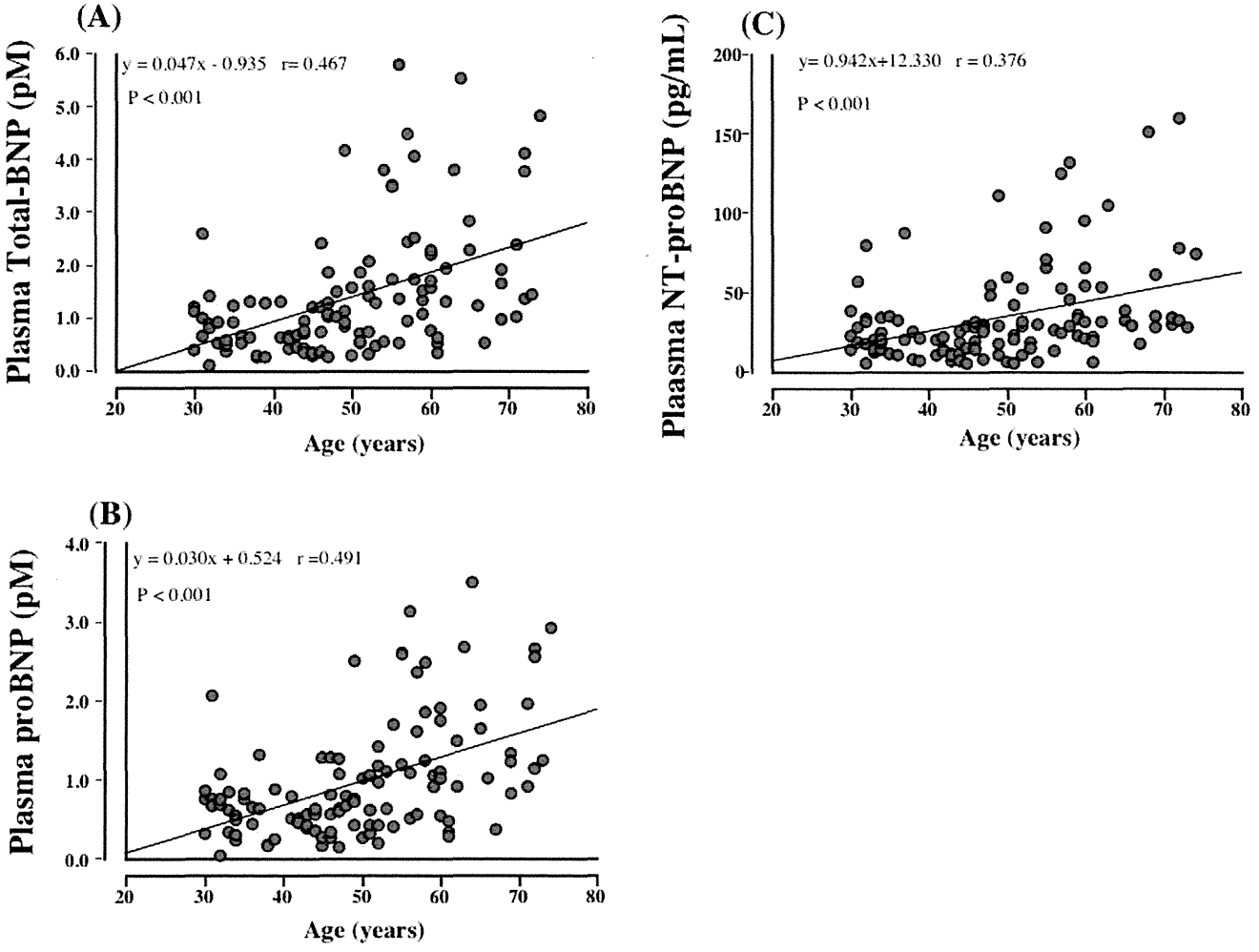

Figure 5. The relationships between total BNP (A), proBNP (B), and NT-proBNP (C) and age.
doi:10.1371/journal.pone.0053233.g005

ratios are higher in heart failure patients with ventricular overload than those with atrial overload [6]. Although this protocol provides useful information, the methodology is time-consuming and impractical for routine assays in clinical laboratories. In addition, recovery of proBNP may be diminished by both extraction and the gel filtration steps [9,16]. To overcome these problems, we developed new direct immunochemiluminescent assays for proBNP and total BNP.

We used two monoclonal antibodies, BC203 and 18H5, to assay proBNP. BC203 recognizes an epitope in the C-terminal of proBNP, while 18H5 recognizes an epitope in the N-terminal. Recent studies showed that proBNP has seven sites suitable for *O*-linked oligosaccharide attachment (Ser36, Thr37, Thr44, Thr48, Thr53, Ser58 and Thr71) within the N-terminal portion of the peptide [14]. Because the *O*-linked oligosaccharide attachments almost completely inhibit the binding of the antibody to the peptide [17], we selected 18H5, which recognizes the N-terminal of proBNP (a.a. 13–20) in a region not subject to glycosylation (Figure 1). To assay total BNP, we used the monoclonal antibodies BC203 and KY-BNP-II, as previously reported [10]. In both assays, BC203 served as the capture antibody. Importantly, because the affinity of 18H5 for the N-terminal portion is similar to the affinity of KY-BNP-II for the ring structure, we are able to calculate the proBNP/total BNP ratio. In addition, our new assays are less time-consuming and more sensitive and accurate than earlier ones, and the lower detection limits for total BNP (0.02 pmol/L) and proBNP (0.04 pmol/L) enabled us to measure plasma proBNP levels in nearly all the healthy subjects tested.

We used gel-filtration on two tandemly connected Superdex 75 columns to determine the molecular mass of plasma proBNP. As shown in Figure 3-A,B, a single peak of proBNP was obtained in both the total BNP and proBNP assay systems. The elution points are consistent with that of glycosylated proBNP, but not deglycosylated proBNP, and deglycosylation treatment significantly shifted the peak rightward (Figure 3-A,B) to an elution point consistent with proBNP. The peak immunoreactivity of proBNP after deglycosylation was slightly smaller than before treatment, suggesting the recovery rate of proBNP after gel-filtration is lower than that of glycosylated proBNP, which is consistent with proBNP being more adsorptive than glycosylated proBNP. Our findings are also consistent with previous Western blot analyses showing that plasma levels of glycosylated proBNP are elevated and no substantial level of proBNP is detected in severe heart failure [7]. Taken together, these results suggest that the major molecular form of proBNP in the plasma of patients with heart failure is the glycosylated form.

ProBNP is also the important molecular form of BNP in the plasma of healthy subjects. When we previously used gel-filtration

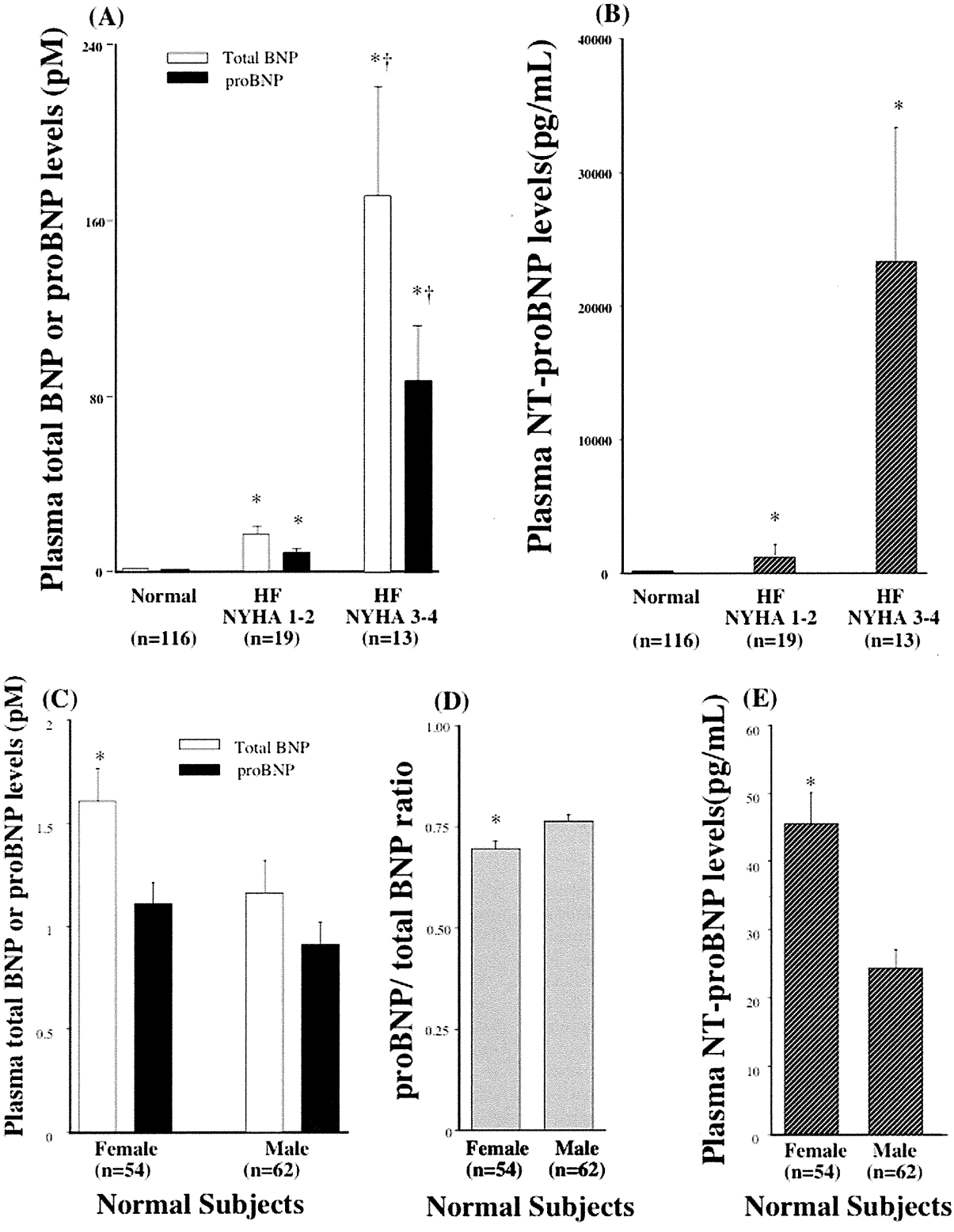

Figure 6. Plasma Levels of proBNP, total BNP, and NT-proBNP in normal and heart failure. Bar graph showing the total BNP, proBNP (A) and NT-proBNP (B) levels in healthy subjects and heart failure patients with NYHA classes 1–2 and 3–4. *P<0.05 vs total BNP and proBNP in normal, †P<0.05 vs total BNP and proBNP in HF NYHA 1–2. Bar graph showing the total BNP, proBNP (C), proBNP/total BNP ratio (D) and NT-proBNP (E) levels in male and female in healthy subjects. Values are means ± SE. *P<0.05 vs male.
doi:10.1371/journal.pone.0053233.g006

and a fluorescent immunoenzyme assay to measure BNP and proBNP, we found that levels of BNP were slightly higher than those of proBNP in both healthy subjects and heart failure patients. The exact reason for the discrepancy in proBNP levels between the earlier study and the present one is unclear; however, the lower recovery caused by the need for extraction from plasma on a Sep-Pak C18 cartridge may have contributed to the lower proBNP levels in the earlier study [9,16]. Recent studies have shown that proBNP has much less ability to induce cGMP production in vascular smooth muscle and endothelial cells than BNP [7,18]. This suggests that increases in the levels of the low-activity proBNP in heart failure may contribute to the so-called "BNP paradox" [19]. That is, administration of exogenous recombinant human BNP to heart failure patients has a substantial clinical and hemodynamic impact, despite the presence of high levels of immunoreactive BNP in their plasma, as measured with commercially used BNP assays.

In the current study, we showed that total BNP and NT-proBNP increased with aging, which are consistent with the previous studies. In addition, the current study first showed that plasma proBNP level increased with aging. However, there were no statistical differences in NT-proBNP between 30~39 and 50~59, whereas there were significant differences in total and proBNP between 30~39 and 50~59, suggesting that total and proBNP are more sensitive than NT-proBNP. In addition, total and proBNP seemed to be well correlated with age ($r = 0.467$. 0.491, each) than NT-proBNP ($r = 0.376$). Thus, total BNP and proBNP may be better marker in discriminating the effect of age than NT-proBNP. Increased myocardial mass and/or reduction of renal clearance of natriuretic peptides with aging may be one of the possible reason for increased BNP and NT-BNP with aging; however, exact mechanism for it still remains unknown and further study is necessary to investigate the relationships between proBNP and aging.

We also analyzed the effects of gender on proBNP, total BNP, proBNP/total BNP ratio and NT-proBNP. Interestingly, in female higher total BNP and NT-proBNP and lower proBNP/total BNP ratio without changing of proBNP was observed. Calculated BNP (total BNP - proBNP) was also increased. This finding may be explained that increased proBNP production and higher processing rate. Further study is necessary to elucidate the mechanism of increased total BNP and NT-proBNP and lower proBNP/total BNP ratio without changing of proBNP in female.

In summary, we have developed rapid and precise immunochemiluminescent assay systems for routine determination of total BNP and proBNP levels in human plasma. Using these assay systems we showed that in addition to BNP, considerable amount of proBNP circulates in both healthy subjects and heart failure patients. The precise relation of the proBNP/total BNP ratio to heart failure remains unknown, as does whether the heart mainly secretes proBNP. Likewise, the effects of age, sex and renal function on proBNP levels remain unknown. We anticipate our new assays for the proBNP and total BNP will be helpful for addressing each of those issues.

Acknowledgments

We thank Ms. Aoi Fujishima and Masako Matsubara for her excellent technical assistance and Ms.Yukari Kubo for her excellent secretarial work.

Author Contributions

Gave useful comments and discussion: K. Kamgawa K. Nakao. Conceived and designed the experiments: TN HO NM KH. Performed the experiments: MN NO K. Nagata. Analyzed the data: YN HK CY K. Nakao. Contributed reagents/materials/analysis tools: TM YK K. Koichiro IM. Wrote the paper: TN HO.

References

1. Maisel AS, Nakao K, Ponikowski P, Peacock WF, Yoshimura M, et al. (2011) Japanese-Western consensus meeting on biomarkers. Int Heart J. 52:253–65.
2. Jessup M, Abraham WT, Casey DE, Feldman AM, Francis GS, et al. (2009) ACCF/AHA Guidelines for the Diagnosis and Management of Heart Failure in Adults: a report of the American College of Cardiology Foundation/American Heart Association Task Force on Practice Guidelines: developed in collaboration with the International Society for Heart and Lung Transplantation. Circulation. 119:1977–2016.
3. Dickstein K, Cohen-Solal A, Filippatos G, McMurray JJ, Ponikowski P, et al. (2008) ESC Guidelines for the diagnosis and treatment of acute and chronic heart failure 2008: the Task Force for the Diagnosis and Treatment of Acute and Chronic Heart Failure 2008 of the European Society of Cardiology. Developed in collaboration with the Heart Failure Association of the ESC (HFA) and endorsed by the European Society of Intensive Care Medicine (ESICM). ESC Committee for Practice Guidelines (CPG). Eur Heart J. 29:2388–442.
4. Minamino N, Horio H, Nishikimi T (2006) Chapter 165. Natriuretic peptides in the cardiovascular system. In: Kastin AJ, editor. THE HANDBOOK OF BIOLOGICALLY ACTIVE PEPTIDES. 1st ed. Academic Press, pp. 1217–1225
5. Waldo SW, Beede J, Isakson S, Villard-Saussine S, Fareh J, et al. (2008) Pro-B-type natriuretic peptide levels in acute decompensated heart failure. J Am Coll Cardiol. 51:1874–82.
6. Nishikimi T, Minamino N, Ikeda M, Takeda Y, Tadokoro K, et al. (2010) Diversity of molecular forms of plasma brain natriuretic peptide in heart failure–different proBNP-108 to BNP-32 ratios in atrial and ventricular overload. Heart. 96:432–9.
7. Liang F, O'Rear J, Schellenberger U, Tai L, Lasecki M, et al. (2007) Evidence for functional heterogeneity of circulating B-type natriuretic peptide. J Am Coll Cardiol. 49:1071–8.
8. Nishikimi T, Minamino N, Horii K, Matsuoka H (2007) Do commercially available assay kits for B-type natriuretic peptide measure Pro-BNP1-108, as well as BNP1-32? Hypertension. 50:e163
9. Semenov AG, Seferian KR (2011) Biochemistry of the human B-type natriuretic peptide precursor and molecular aspects of its processing. Clin Chim Acta. 412:850–60
10. Tsuji T, Inouye K, Yamauchi A, Kono M, Igano K (2004) U.S. Patent 6, 677, 124 B2, pp 16, Shionogi Seiyaku Kabushiki Kaisha, Japan.
11. Seferian KR, Tamm NN, Semenov AG, Tolstaya AA, Koshkina EV, et al. (2008) Immunodetection of glycosylated NT-proBNP circulating in human blood. Clin Chem. 54:866–73.
12. Ishikawa E, Imagawa M, Hashida S, Yoshitake S, Hamaguchi Y, et al. (1983) Enzyme-labeling of antibodies and their fragments for enzyme immunoassay and immunohistochemical staining. J Immunoassay. 4:209–327.
13. Nishikimi T, Ikeda M, Takeda Y, Ishimitsu T, Shibasaki I, et al. (2012) The effect of glycosylation on plasma N-terminal proBNP-76 levels in patients with heart or renal failure. Heart. 98:152–61
14. Schellenberger U, O'Rear J, Guzzetta A, Jue RA, Protter AA, et al. (2006) The precursor to B-type natriuretic peptide is an O-linked glycoprotein. Arch Biochem Biophys. 451:160–6.
15. Nishikimi T, Kuwahara K, Nakao K. (2011) Current biochemistry, molecular biology, and clinical relevance of natriuretic peptides. J Cardiol. 57:131–40.
16. Seferian KR, Tamm NN, Semenov AG, Mukharyamova KS, Tolstaya AAet al. (2007) The brain natriuretic peptide (BNP) precursor is the major immunoreactive form of BNP in patients with heart failure. Clin Chem. 53:866–73.
17. Hammerer-Lercher A, Halfinger B, Sarg B, Mair J, Puschendorf B, et al. (2008) Analysis of circulating forms of proBNP and NT-proBNP in patients with severe heart failure. Clin Chem. 54:858–65.
18. Heublein DM, Huntley BK, Boerrigter G, Cataliotti A, Sandberg SM, et al. (2007) Immunoreactivity and guanosine 3′,5′-cyclic monophosphate activating actions of various molecular forms of human B-type natriuretic peptide. Hypertension. 49:1114–9.
19. Menon SG, Mills RM, Schellenberger U, Saqhir S, Protter AA (2009) Clinical implications of defective B-type natriuretic peptide. Clin Cardiol. 32:E36–41.

Kondo *et al. Molecular Brain* 2011, **4**:27
http://www.molecularbrain.com/content/4/1/27

Molecular Brain

RESEARCH Open Access

Long-term changes of spine dynamics and microglia after transient peripheral immune response triggered by LPS *in vivo*

Satoru Kondo[1*], Shinichi Kohsaka[2] and Shigeo Okabe[1]

Abstract

Background: An episode of peripheral immune response may create long-lasting alterations in the neural network. Recent studies indicate a glial involvement in synaptic remodeling. Therefore it is postulated that both synaptic and glial changes could occur under the peripheral inflammation.

Results: We tested this possibility by *in vivo* two-photon microscopy of dendritic spines after induction of a peripheral immune response by lipopolysaccharide (LPS) treatment of mice.
We observed that the spines were less stable in LPS-treated mice. The accumulation of spine changes gradually progressed and remained low over a week after LPS treatment but became significantly larger at four weeks. Over eight weeks after LPS treatment, the fraction of eliminated spines amounted to 20% of the initial population and this persistent destabilization resulted in a reduction of the total spine density.
We next evaluated glial activation by LPS administration. Activation of microglia was confirmed by a persistent increase of Iba1 immunoreactivity. Morphological changes in microglia were observed two days after LPS administration and were partially recovered within one week but sustained over a long time period.

Conclusions: These results indicate long-lasting aggravating effects of a single transient peripheral immune response on both spines and microglia. The parallel persistent alterations of both spine turnover and the state of microglia *in vivo* suggest the presence of a pathological mechanism that sustains the enhanced remodeling of neural networks weeks after peripheral immune responses. This pathological mechanism may also underlie long-lasting cognitive dysfunctions after septic encephalopathy in human patients.

Keywords: Peripheral inflammation, Spine, Microglia, *in vivo* imaging, Sepsis

Background

Sepsis is a serious medical condition caused by a severe immune response to infection. Recent studies have demonstrated that patients recovered from septic conditions can have long-term cognitive impairment, including memory deficits and attention disorders [1]. How impairment of brain functions persists long after recovery from sepsis still remains to be poorly understood. Peripheral injection of bacterial lipopolysaccharide (LPS), endotoxin from gram-negative bacteria, mimics the pathological state of sepsis. LPS interacts with Toll-like receptors on macrophages and initiates production of a variety of proinflammatory cytokines including tumor necrosis factor (TNF)- α, interleukin (IL)-1β, and IL-6 [2,3]. These cytokines cross the blood-brain barrier, activate cells of the brain capillaries, and also activate vagal afferents. Subsequently, these responses further induce the synthesis of prostaglandins [4-6] and cytokines within the brain that cause fever and general feelings of illness [7].

Consistent with cognitive impairment in human subjects who recovered from sepsis, peripheral administration of LPS in rodents has been shown to affect cognitive functions [8]. In line with these findings, LPS has also been demonstrated to impair long-term potentiation (LTP), a key cellular process in learning and memory

* Correspondence: kondo@med.kyushu-u.ac.jp
[1]Department of Cellular Neurobiology, Graduate School of Medicine, University of Tokyo, Bunkyo-ku, Tokyo 113-0033, Japan
Full list of author information is available at the end of the article

[9,10]. How does LPS-evoked peripheral inflammation affect functions of the neural network? One obvious possibility is through alterations of glia [11]. Microglial cells are resident immune cells in the CNS [12,13] and have the ability to respond to inflammation by changing their shape from ramified to amoeboid morphology [14] or by changing the expression profile of marker molecules, such as ionized calcium binding adaptor molecule 1 (Iba1) [15,16]. Recent *in vivo* imaging studies reported rapid motility of microglial processes [17,18]. Direct contact of microglia with synapses may also be involved in synapse stripping in pathological conditions [19].

The neuronal network in the mammalian forebrain has been shown to be intrinsically dynamic [20,21] and *in vivo* time-lapse two-photon microscopy of dendritic spines in the mouse neocortex has provided direct evidence of network remodeling [22,23]. Although previous *in vivo* imaging studies reported remodeling of synapses after induction of ischemia [24,25] and in neurodegenerative conditions [26,27], long-lasting changes of synapses triggered by peripheral inflammatory responses have not yet been investigated. Here we performed *in vivo* spine imaging after LPS treatment. Surprisingly, mild and transient peripheral inflammation induced long-lasting changes of spine dynamics, associated with persistent up-regulation of Iba1 expression in microglia. The parallel sustained alterations of both spine turnover and the state of microglia *in vivo* may underlie long-term cognitive impairment after septic encephalopathy in human patients.

Methods

Animals

All experimental procedures were carried out in compliance with the institutional guidelines of the University of Tokyo and the government. This study was approved by the animal welfare ethics committee at the University of Tokyo, Faculty of Medicine with the approval ID of P08-016. Every effort was made to minimize the suffering and the number of animals used.

For *in vivo* imaging and histochemical analyses, both male and female C57BL/6 transgenic mice aged two to three months were used. For *in vivo* spine imaging, transgenic mice expressing green fluorescence protein (GFP) under the control of the *Thy1* promoter (*Thy1-GFP* M mice) were used [28]. To visualize microglia, transgenic mice expressing GFP under the control of the *Iba1* promoter (*Iba1-GFP* mice) were used [29].

Drug treatment

E.coli lipopolysaccharide (LPS, strain O111:B4, Sigma-Aldrich (catalog number L4391)) was dissolved in a saline solution at a concentration of 0.2 mg/mL and stored at -30°C in small aliquots. Mice were intraperitoneally injected with a single dose of LPS (0.5 mg/kg). The optimal dose of LPS was determined from the morphological changes in microglia two days after LPS injection with doses of 0.1, 0.3, 0.5 or 5.0 mg/kg. We observed morphological changes in microglia at doses higher than 0.5 mg/kg. Injection of LPS at 5.0 mg/kg induced severe behavioral responses, while sickness behavior was less prominent at lower doses. From these pilot experiments, we selected a dose of 0.5 mg/kg for experiments with spine imaging and glial activation.

Surgery

Mice were deeply anesthetized intraperitoneally with ketamine (100 mg/kg body weight) and xylazine (10 mg/kg body weight) diluted in a saline solution. After the disappearance of the pinching response the hair of the scalp was shaved and a midline incision of the scalp was made. Periosteum tissue was removed with a surgical blade and the somatosensory area (-1.5 mm from Bregma and 2.0 mm from the midline) was marked by stereotactic coordinates. A small rectangular metal plate with a round hole was glued on the skull and mice were fixed to the immobilized stage (SR-5M, Narishige) with a heating pad to maintain body temperature. The skull above the imaging area was thinned through the round hole of the metal plate. The thinning was initially done over a small area (a 1.5 × 1.5 mm square) with a high speed micro-drill (KM11, Minimo). When the bone reached ~50 μm in thickness, further thinning was performed manually with micro surgical blades (NORDLAND blade, Salvin Dental) until the skull reached ~15 μm in thickness. We paid particular attention not to push the skull during the thinning process. The final imaging window was a 0.5 × 0.5 mm square. For the repetitive imaging, the brain vasculature pattern was recorded with a CCD camera (GZ-MG70, Victor).

In vivo imaging

A scanning microscope (FV-300, Olympus) equipped with a pulsed laser (MaiTai HP, Spectra Physics) was used for imaging with a water immersion objective lens (1.05 NA, 25x, Olympus). The wavelength was 920 nm and the average power of the laser after the objective lens was between 10 and 20 mW. The imaging area was 234 μm × 234 μm (low magnification) or 78 μm × 78 μm (high magnification), with an imaging depth 50 μm from the surface of the neocortex (Layer 1) and the step size of the z stack set to 0.75 μm. The pixel sizes of single horizontal images were set to 512 × 512. Low magnification images, together with images of the vasculature pattern taken with a CCD camera, served as the reference maps for repetitive acquisition of higher magnification images from the same cortical area. For

repeated imaging, the metal plate attached on the skull was removed and the skin was sutured. The mice were kept on the heating pad until they recovered from the anesthesia and were returned to their home cage. To minimize the damage to the brain tissue due to the re-thinning of the skull, mice were imaged twice for most of the experiments and three times at the maximum.

Fixation of animals and immunohistochemistry

Wild type or *Iba1-GFP* mice were sampled before or two, seven, 28 days after LPS injection. Mice were deeply anesthetized with pentobarbital and perfused transcardially with PBS followed by 4% paraformaldehyde. Brains were removed and further fixed in 4% paraformaldehyde overnight at 4°C. Slices were made with a vibratome (DTK-1000, Dosaka EM) with a 50 μm thickness. Slices from wild type mice were stained with anti-Iba1 antibody (1/500, Wako Pure Chemicals) or anti-glial fibrillary acidic protein (GFAP) antibody (1/3000, Sigma-Aldrich) followed by the fluorescence conjugated secondary antibodies to visualize the microglia or astrocytes. Mice from various time intervals after LPS injection or control were fixed on the same day and slices were stained at the same time. Images were obtained by using a laser scanning confocal microscope (FV-1000, Olympus) or a wide-field fluorescence microscope (BX-50, Olympus) under the same illumination and collection conditions.

Data analysis

All analyses of spine dynamics, densities, and estimations of sizes were done manually using National Institutes of Health ImageJ software (http://rsb.info.nih.gov/ij). We could identify both spines and filopodia [30] but analyzed only dendritic protrusions classified as spines in this study (Figure 1) [31]. The same dendritic segments (5-50 μm length) were identified from the image stacks at different time points and spines were selected and classified into three groups. New spines were those identified only at the second time point. Eliminated spines were those present only at the first time point but missing at later points. Spines present at both time points were categorized as stable spines. The number of spines in each group was counted and both the formation and elimination rates were calculated as the percentages of eliminated spines and newly formed spines to the total number of spines examined respectively. To ensure the tissue movements and rotations three-dimensional stacks were always used for the analysis. We did not analyze structures that projected mainly along the imaging axis, below or above dendrites. We considered a spine in the second image to be the same spine as in the first image if the second image spine was located within 0.5 μm of the expected location based on its spatial relationship to adjacent spines or landmarks like axonal and dendritic orientation.

For the morphological analysis of spines, we selected dendritic segments where eliminated spines could be identified. Binary images were constructed by appropriate thresholding to determine the outline of spines. The length from the neck to the tip of a spine (a) and the maximum width of a head (b) were measured manually and the sum of these two values was taken as a parameter reflecting spine size.

For the spine density analysis, we used the same dendritic segments as in the spine turnover analysis. We selected the dendritic segments whose lengths were more than 20 μm for the spine density calculation. Spine density was calculated as (N of spines)/(lengths of dendritic segments).

For the analysis of Iba1 expression we took 41 images at the z step of 1 μm and a maximum projection image was generated from the same number of stack images for all the individual slices. Images were obtained with a laser scanning confocal microscope (FV-1000, Olympus) under the same illumination and collection conditions. The total fluorescence intensity of projection image was measured by ImageJ software. The background intensity was subtracted from the total fluorescence intensity. The intensity values were normalized to the mean intensity value of the control.

The density of microglia was calculated from the same slices as used for the measurement of intensity. The number of Iba1-positive cell bodies was manually counted three-dimensionally from 41 image stacks. The number of microglia was normalized to the mean number of microglia in the control.

Imaris v6.1.3 (Bitplane, Zurich, Switzerland) was used for the three-dimensional analysis of microglial processes. Surface rendering of GFP-positive microglia from z-stacks of confocal microscope images was performed and the lengths of processes were determined by measuring the distance from the centroid of a cell body to the tip along the processes.

Structural dynamics of microglia were quantified from time-lapse imaging of soma and protrusions *in vivo*. Images were obtained every three min for 30 min. We took 51 images at the z step of one μm for each time-interval image. The analysis was performed on maximum-intensity projections of fluorescence image stacks. The same number of stack images was used for each cell analysis. The dynamics of microglia were evaluated by measuring the length of extension and retraction of microglial protrusions. Ten processes of microglia were randomly selected and the length of extension and retraction was measured to compare the overlay of two images at two different time points.

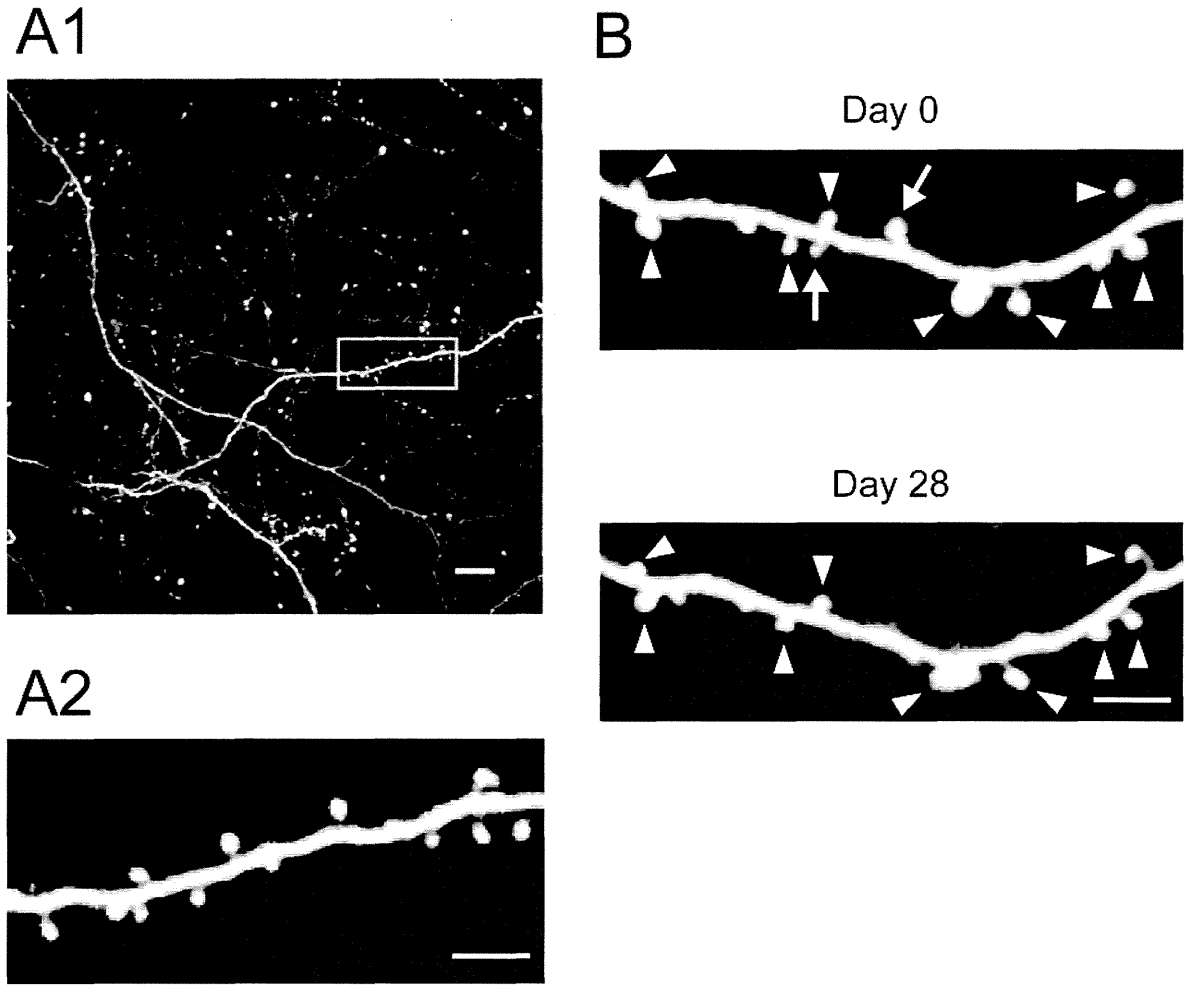

Figure 1 Two-photon microscopy of dendritic spines. (A1) Typical morphologies of dendrites in the superficial layer of the neocortex detected by *in vivo* two-photon microscopy. This is a projection image of z-stacks. Scale bar, 10 μm. (A2) Higher magnification view of the dendritic segment marked by the rectangle in A1. The image was generated from a montage of several adjacent optical sections separated by 0.75 μm in the Z-direction. Scale bar, 5 μm. (B) *In vivo* imaging of dendritic segments at two time points (day 0 and day 28). These images were also generated from a montage of several adjacent optical sections separated by 0.75 μm in z-direction, illustrating stable spines (arrowheads) and eliminated spines (arrows). Scale bar, 5 μm.

All the data are presented as means ± S.D. Multiple comparisons were made by an ANOVA test, followed by a Tukey's test (Figures 2, 3, 5, 6, 7). Statistical significance was evaluated using Student's t-test (Figure 4). Differences were considered to be significant if $p < 0.05$.

Cytokine array analysis

Tissue extracts from control and LPS-treated mice were screened by using a cytokine antibody array kit (Array1, RayBiotech Inc., Atlanta, GA, USA) according to the manufacturer's instructions. After euthanasia of mice with a large dose of pentobarbital, the neocortex and the hippocampus were dissected from the forebrain and homogenized in a lysis buffer. Brain extracts were then centrifuged at 10,000 × g for 10 min at 4°C. Protein concentrations of supernatants were determined and equal amounts of protein were incubated with array membranes. The signals generated by enhanced chemiluminescence were recorded by ChemiDoc XRS (Bio-Rad, Tokyo, Japan). For the analysis of chemiluminescence signals from cytokine spots, total signals were calculated and then background intensity was subtracted. The averaged optical densities of the six positive controls on the membrane were calculated and the optical densities of cytokine spots were divided by these values. These normalized values were compared and the ratio between control and LPS-treated mice was calculated.

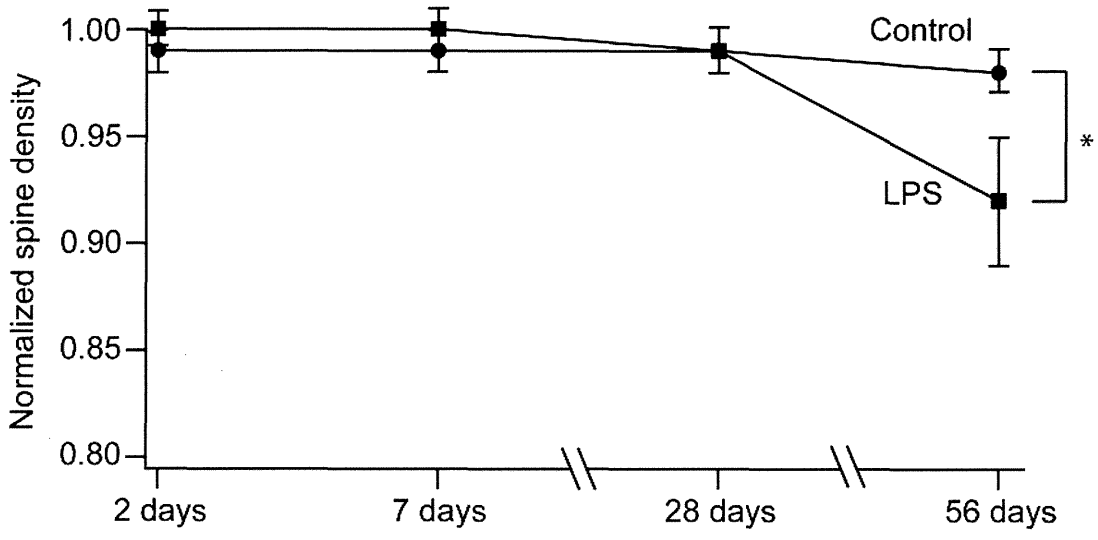

Figure 2 Temporal change of spine density after LPS treatment. Average spine densities at different time points after LPS treatment were calculated and normalized against the value at day zero (before LPS administration in the LPS-treated group). Spine densities were maintained close to the original value until 28 days after LPS injection. However, there was a late decline of spine density in LPS-treated group and the difference was statistically significant (*, $p < 0.05$).

Results

Transient peripheral immune response induces long-lasting changes of spine dynamics *in vivo*

Turnover of excitatory synapses in the neocortex with or without stimulation of the peripheral immune system can be quantitatively evaluated by two-photon imaging of dendritic spines *in vivo*. We visualized apical dendrites of pyramidal neurons in the somatosensory cortex of adult transgenic mice expressing GFP under the control of the *Thy1* promoter in a small subset of the CNS neurons (*Thy1-GFP* M mice) [28]. We selected the thinned-skull method in this study, because of the less prominent effects of this surgical procedure on the activation of glial cells [32]. To detect spines generated and eliminated, we obtained image stacks of GFP-filled dendrites by two-photon microscopy at two time points separated by two days, seven days, four weeks or eight weeks (Figure 1A). A pair of image stacks was compared and spines present in both image stacks, and those present only at a single time point were identified manually (Figure 1B). After identification and classification of spines, the fractions of newly formed spines and eliminated spines were calculated. The fraction of spines added or eliminated in unperturbed animals was low and comparable to a previous report [33]. The fraction of dynamic spines was less than 5% over a period of seven days, 5% over four weeks, and still less than 10% over a period of eight weeks (see Figure 3B).

We challenged *Thy1-GFP* M mice with peripheral administration of LPS and measured the turnover rate of spines. The dose of LPS (0.5 mg/kg) was set to the minimal dose sufficient for up-regulation of Iba-1, which is a well-characterized marker of microglial activation. The protocols for imaging were set to be identical for control and LPS-treated groups, except that the LPS-treated group received a single intraperitoneal injection of LPS after acquisition of spine images on the first day. We first determined if there were any alterations in spine densities after LPS administration (Figure 2). Spine densities (estimated from images taken over intervals from two days to four weeks within the same volume of the cortex) did not show prominent differences, with a tendency for a slight decline [33,34]. However, there was a significant reduction in spine density at eight weeks after LPS treatment, indicating a late impact of LPS treatment on the cortical network.

Delayed changes in the total spine density may be derived from persistent changes in the spine addition/elimination rates triggered by LPS. To test this possibility, we calculated the fractions of added or eliminated spines (Figure 3A). Within the first week after LPS treatment, these dynamic fractions were not significantly larger than the corresponding fractions in the control group (Figure 3B). However, when we waited for four weeks, the fractions of added or eliminated spines accumulated after LPS treatment were significantly larger than the corresponding fractions in the control group (5.5% (control) versus 11.0% (LPS-treated) for spine elimination, 5.2% (control) versus 10.7% (LPS-treated) for spine formation at four weeks). Spine elimination was further enhanced by LPS treatment when we waited for eight weeks (7.2% (control) versus 20.9%

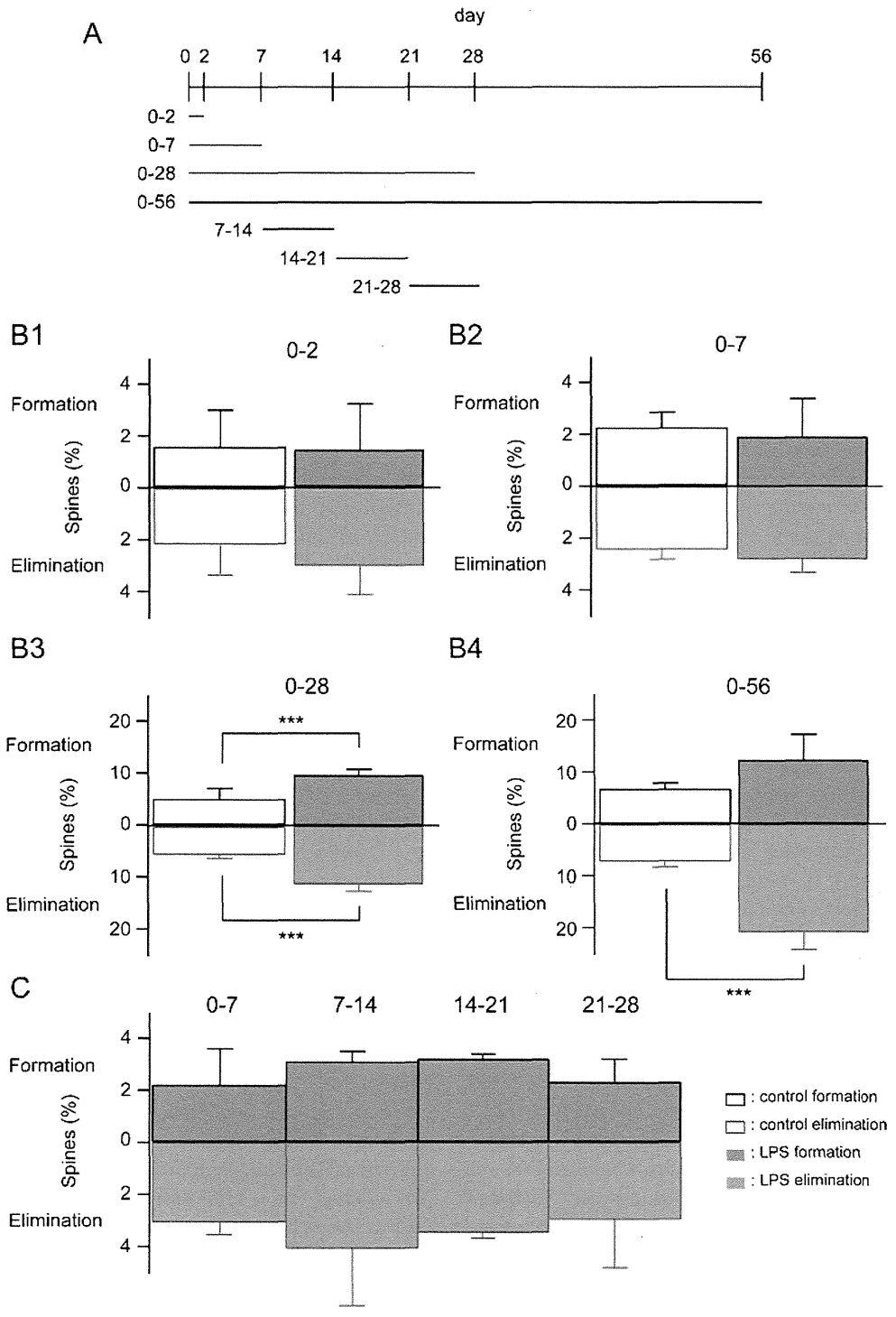

Figure 3 Persistent up-regulation of spine turnover in mice treated with LPS. (A) Spine turnover rates were measured as illustrated in the scheme. (B) Spine turnover rates of control and LPS-treated mice measured at two, seven, 28, and 56 days. Upward bars (black) and downward bars (red) represent the formation and elimination rate of spines, respectively. Spines formed and eliminated in control: 2.4 ± 1.4% and 2.5 ± 1.1% over two days (N = 6) (B1), 2.6 ± 0.4% and 2.7 ± 0.6% over seven days (N = 6) (B2), 5.2 ± 2.1% and 5.5 ± 0.6% over 28 days (N = 6) (B3), 6.8 ± 1.1% and 7.2 ± 1.1% over 56 days (N = 3) (B4). Spines formed and eliminated after LPS injection: 1.7 ± 1.8% and 3.3 ± 1.1% over two days (N = 3) (B1), 2.2 ± 1.4% and 3.1 ± 0.5% over seven days (N = 3) (B2), 10.7 ± 1.5% and 11.0 ± 1.2% over 28 days (N = 6) (B3), 12.4 ± 4.9% and 20.9 ± 3.5% over 56 days (N = 4) (B4). These data were statistically compared between control and LPS treatment (spines formed: $p > 0.5$ for two days; $p > 0.5$ for seven days; $p < 0.001$ for 28 days; $p > 0.1$ for 56 days; spines eliminated: $p > 0.1$ for two days; $p > 0.1$ for seven days; $p < 0.001$ for 28 days; $p < 0.001$ for 56 days). ***, $p < 0.001$. (C) Spine turnover measured with a fixed interval but with different days of the first imaging.

(LPS-treated)), but the extent of spine addition did not match that of elimination in the LPS-treated group (6.8% (control) versus 12.4% (LPS-treated)). This unbalance of addition and elimination of spines could explain the reduction of the total spine density at eight weeks after LPS treatment.

The selective increase of the dynamic spine fraction at late time points could be explained by either an accumulation of small changes gradually over time or by abrupt up-regulation of dynamics at specific time points. To discriminate between these two possibilities, we imaged dendritic spines with intervals fixed to one week, but altered the first imaging days to be either zero, seven, 14, or 21 days after LPS treatment. We could not detect up-regulation of spine dynamics in any of these time segments (Figure 3C), supporting the first possibility that the accumulation of small changes only becomes obvious four weeks after LPS treatment. In other words, these results indicate the presence of persistent alterations in spine dynamics lasting well beyond several weeks after transient and mild activation of the peripheral immune system.

Morphological characteristics of eliminated spines

Next, we evaluated morphological characteristics of spines eliminated early (within one week) or late (later than four weeks) after the initial time point of the spine imaging. Previous reports on spine lifetime in slices indicated that spines with larger volumes had longer lifetimes [35]. Therefore, small spines may have a higher probability for elimination after LPS treatment *in vivo*. On the other hand, if spine elimination is a stochastic process with no preference for size, we might not detect any differences in spine size between groups with different lifetimes. To discriminate between these possibilities, we evaluated the morphology of individual spines by calculating the sum of their lengths and widths (Figure 4A). This measurement suggests that indeed there exists differences in morphology between spines eliminated within one week and those that remained (Figure 4B1). Eliminated spines tended to be smaller than the stable ones ($p < 0.001$). However, a similar comparison between spines eliminated within one month and those that survived for one month did not show such a tendency (Figure 4B2). Thus, we consider the spines with a life-time of less than a week morphologically distinct from the remaining spine population.

LPS treatment increased the fraction of added and eliminated spines only in a late phase. At four weeks after LPS treatment, the fraction of eliminated spines was 10%, twice as large as the fraction in the control (5%). If LPS treatment affected a subset of spines, such as those with smaller volumes, we might be able to detect changes in the frequency distribution of spines eliminated late after LPS treatment. However, the morphology of spines eliminated within one week or one month was not significantly different between the LPS-treated group and the control group (Figure 4B and 4C), suggesting that there was no preferential impact of LPS treatment on a subset of spines with a specific morphology.

We conclude that spines destined to be eliminated within a week are smaller than the average in both control and LPS-treated conditions. LPS increased the fraction of spines to be eliminated late after LPS treatment, but the morphological difference of this LPS-sensitive fraction could not be detected by comparison of spine images, indicating that the late effect of LPS is to increase the probability of spine elimination irrespective of the spine size.

LPS-induced alterations in glial properties

The *in vivo* imaging of LPS-treated *Thy1-GFP* M mice indicated the presence of persistent alterations in spine dynamics lasting well beyond several weeks after transient activation of the peripheral immune system. Peripheral immune responses can secondarily induce changes in glial components in the CNS, especially in astrocytes and microglial cells [36,37]. We performed immunohistochemistry of the neocortex two, seven and 28 days after LPS treatment to detect activation of astrocytes and microglial cells. We could not detect up-regulation of the astrocytic marker GFAP. However, Iba1, a marker of microglial activation, was up-regulated at all time points examined ($p < 0.001$ for two, seven, 28 days) (Figure 5A and 5B). Notably, up-regulated Iba1 immunoreactivity was maintained even at 28 days after LPS injection. There was also a specific increase of microglial density at 28 days after LPS treatment ($p < 0.01$) (Figure 5C). These results indicate prolonged activation and late proliferation of microglia following a single peripheral administration of LPS.

Peripheral injection of LPS may induce morphological changes of microglia. To test this possibility, we measured the length of microglial processes using a transgenic mouse line expressing GFP in microglia under the control of the *Iba1* enhancer element (*Iba1-GFP* mice) [29]. Cytoplasmic GFP signals from microglia in *Iba1-GFP* mice reflect cellular morphology more precisely than the immunoreactivity of endogenous Iba1, which may reflect both cell shape and intracellular distribution of the protein. There was a transient shrinkage of microglial processes assessed by GFP signal two days after LPS treatment ($p < 0.001$), but the processes showed re-extension at seven and 28 days after LPS treatment (Figure 6). Consistent with the up-regulation of the endogenous *Iba1* gene, GFP expression under the control of the *Iba1* promoter also increased progressively after LPS treatment.

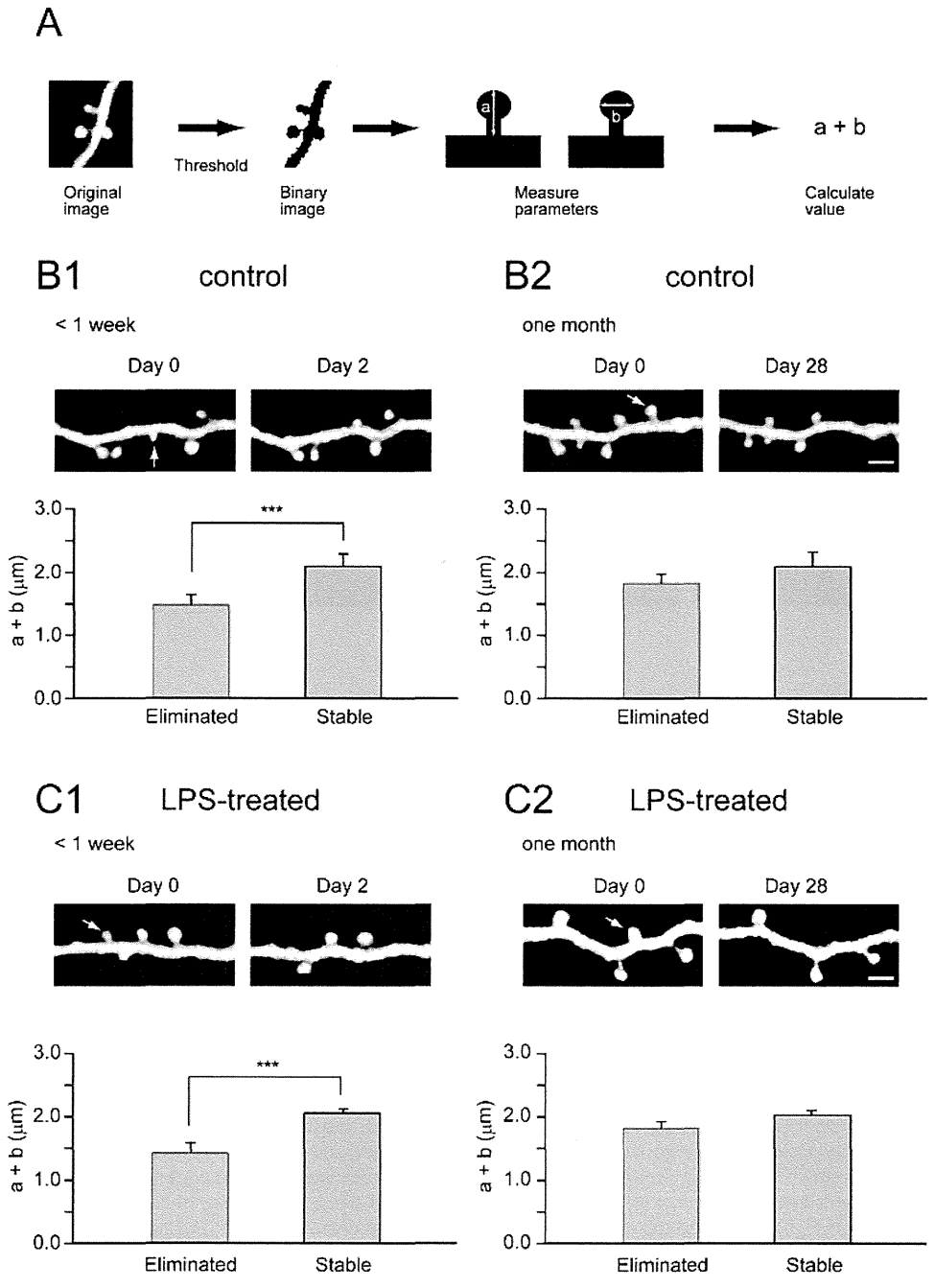

Figure 4 Relationship between spine size and spine elimination. (A) The sizes (both length (a) and width (b)) of spines were measured as illustrated. The sum of the values "a" and "b" was calculated and utilized as an index of spine size. (B1) Spines eliminated within two or seven days were smaller than the spines maintained for the same period. Images are comparisons over two days. An arrow indicates an eliminated spine. The bar graph shows the combined data from images taken over two or seven days, as the frequency distribution of each population was indistinguishable. (B2) When spines were imaged with intervals of 28 days, the sizes of eliminated spines were similar to those of stable spines. An arrow indicates an eliminated spine. (C1) Spines eliminated within two or seven days were smaller than the stable spines also in the LPS-treated group. An arrow indicates an eliminated spine. (C2) Spines eliminated 28 days after LPS treatment had comparable sizes with those maintained. An arrow indicates an eliminated spine. Importantly, the average sizes of eliminated spines between control and LPS-treated groups were not different at two different time points (less than seven days in B1/C1, at 28 days in B2/C2), indicating that the effect of LPS is not selective for a specific size of spines. ***, $p < 0.001$. Scale bars, 2 μm.

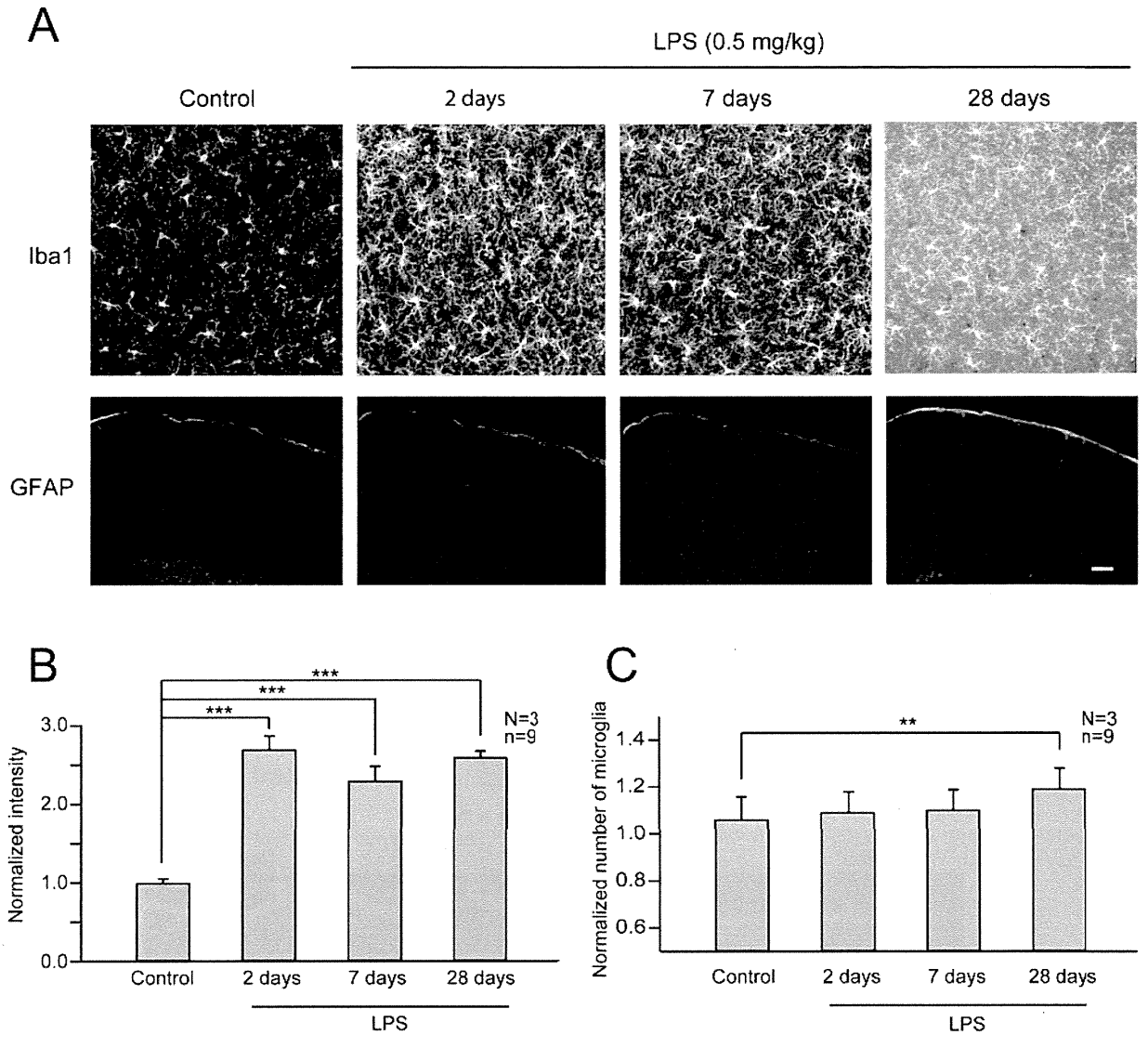

Figure 5 LPS induced persistent activation of microglia. (A) Immunohistochemical analyses were performed with fixed cortical slices from control and LPS treated mice at different time points. Slices were stained either with anti-Iba1 antibody for microglia or anti-GFAP antibody for astrocytes. Projection images are shown. Scale bar in the upper column, 10 μm; bar in the lower column, 400 μm. (B) Temporal profile of enhanced Iba1 expression after LPS treatment. To evaluate expression of Iba1, the total intensity of fluorescence was measured and the averages were plotted as values normalized to the control (N: number of mice, n: number of slices). The intensity of fluorescence was significantly increased after two days of LPS treatment and this increasing trend was maintained until 28 days. (C) Late increase in the number of microglia after LPS treatment. The number of microglia was counted and the averages were plotted as values normalized to the control (N: number of mice, n: number of slices). The number of microglia was significantly increased only at 28 days after LPS treatment. **, $p < 0.01$, ***, $p < 0.001$.

Microglia retracted their processes two days after LPS treatment but recovered from the initial shrinkage of their processes at time points later than seven days. A previous study reported the importance of process motility and contact with synapses for the regulation of synapse remodeling by microglia [19]. To evaluate the extent of microglial process motility, we visualized the dynamics of microglial processes using *in vivo* two-photon microscopy of *Iba1-GFP* mice. Time-lapse images were obtained every three min for 30 min. The temporal profiles of process extension and retraction were created from images of microglia without stimulation (Figure 7A1), microglia two days after LPS treatment (Figure 7A2), and 28 days after LPS treatment (Figure 7A3). The average velocities of process remodeling determined from time-lapse images (Figure 7B) were

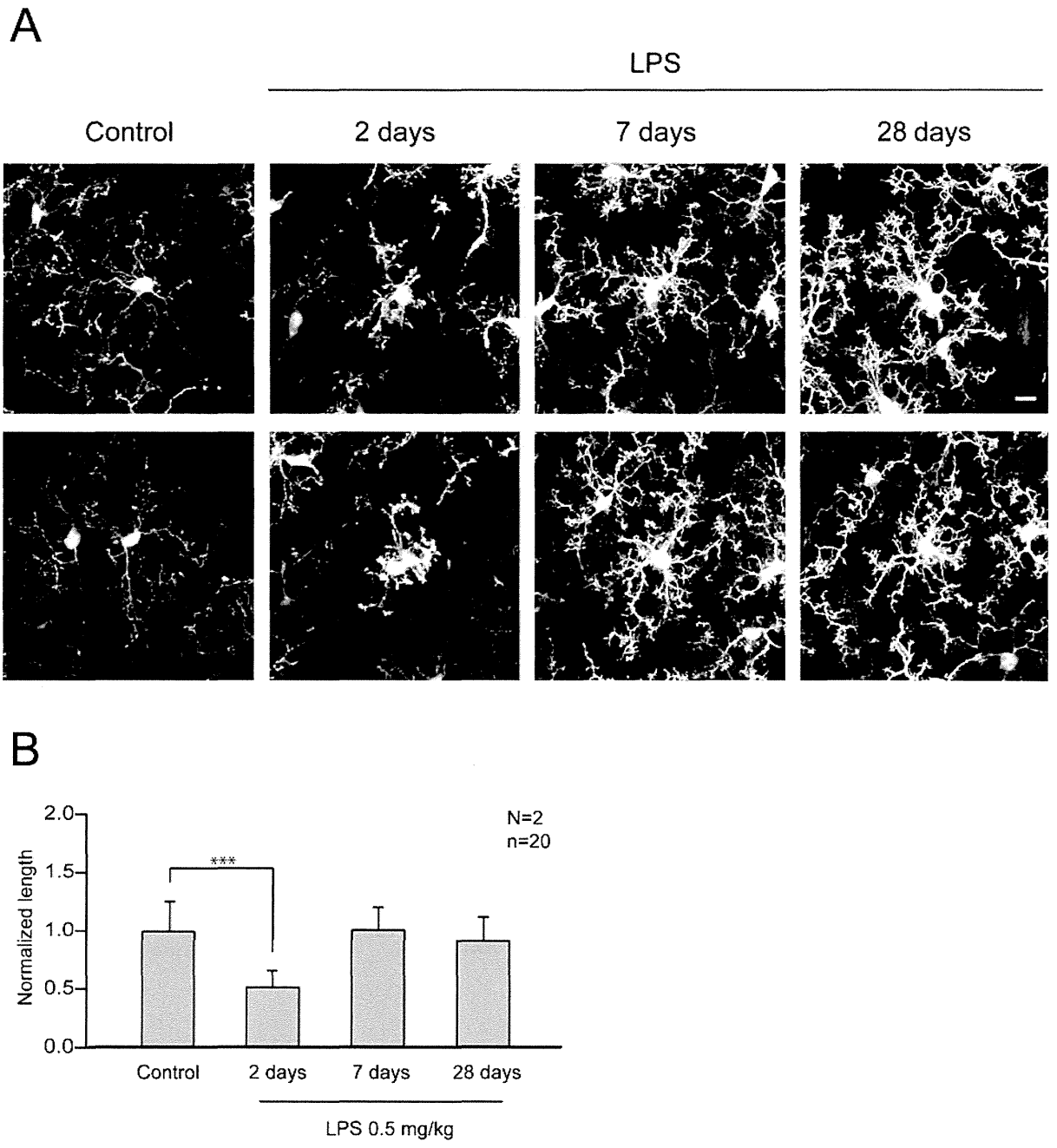

Figure 6 Morphological changes of microglia after LPS treatment. (A) High magnification images of microglia in *Iba1-GFP* mice. Mice were either unperturbed or received LPS injection and were sacrificed for immunohistochemical analyses two, seven, and 28 days later. Scale bar, 10 μm. (B) Total lengths of microglial processes were measured and the averages are shown as lengths normalized to the control (N: number of mice, n: number of microglia). The shrinkage of processes was observed at two days but they recovered their original lengths seven days after LPS injection. GFP signals from the microglial processes were enhanced even at later time points (seven and 28 days), but this may be due to either real increase in process diameters or increases in the GFP protein content. ***, $p < 0.001$.

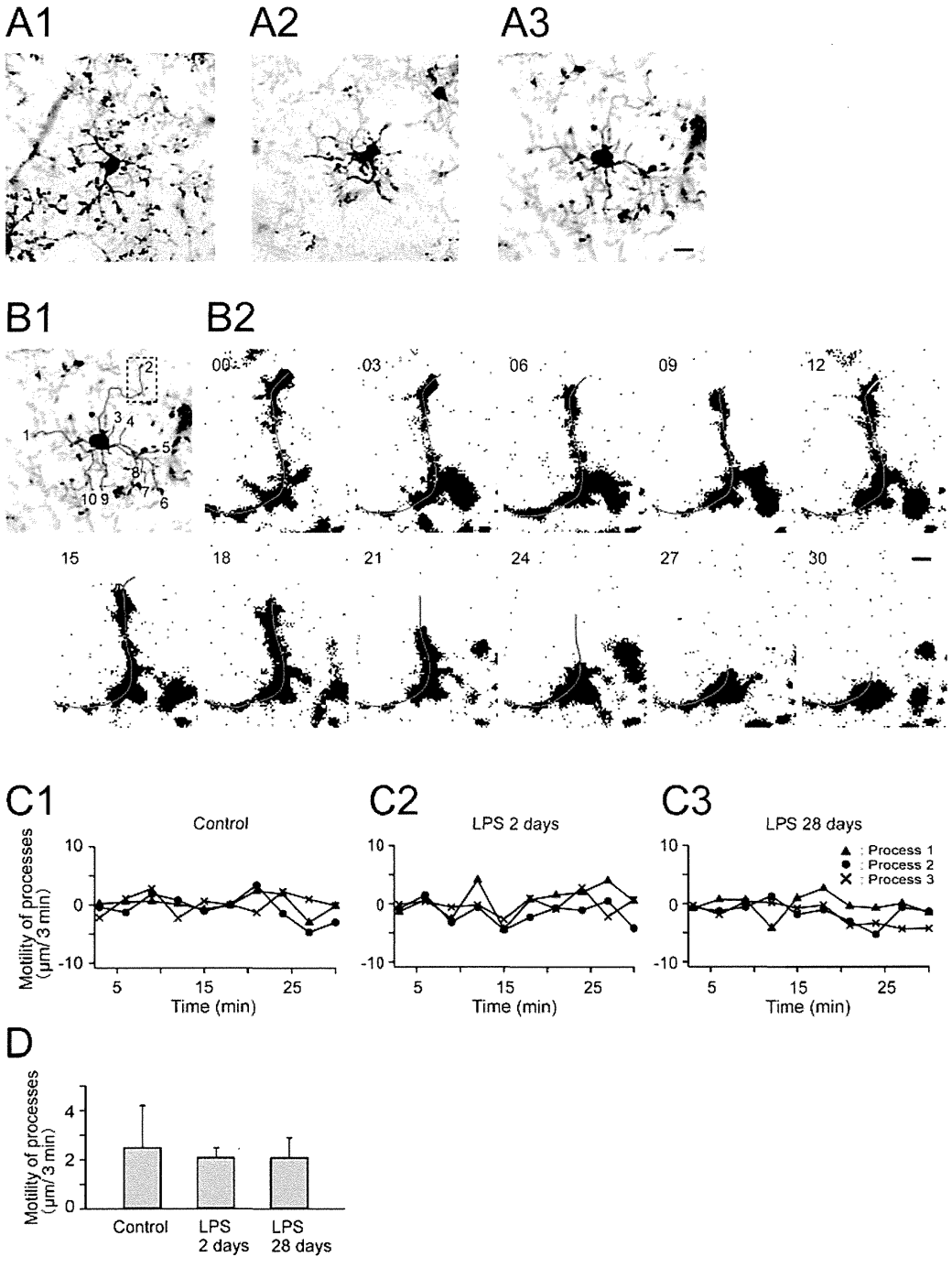

Figure 7 Unaltered dynamics of microglial processes in LPS-treated mice. (A) Morphology of microglia imaged by *in vivo* two-photon microscopy of *Iba1-GFP* mice. A1 shows a cell from a mouse without LPS administration. A2 and A3 show cells from LPS-treated mice at two and 28 days after LPS treatment, respectively. Scale bar, 10 μm. (B1) An example of a microglial cell utilized for time-lapse analysis (identical cell shown in A3). This image shows the morphology at zero time point, with an overlay of green lines (numbered from 1 to 10) on individual processes. The tips of these green lines were recorded and their distances between adjacent time frames (3 min intervals) were calculated as an index of process motility shown in C and D. (B2) Binary images of a microglial process (green line) extracted from time-lapse sequences in the image area marked by a dotted rectangle in B1, illustrating the extent (yellow line) of rapid growth and shrinkage (red line). Numbers in the upper left corner indicate elapsed time in min. Scale bar, 2 μm. (C) The motility of microglial processes. Extension and retraction of processes were plotted for three representative processes with time intervals of three min. Positive values indicate process extension and negative values indicate retraction. (D) Summation of absolute distances of extension and retraction during 30 minutes was calculated and the average speeds per frame (three min) were estimated from 10 processes of control and LPS-treated mice. The average motility was comparable among control and LPS-treated groups.

similar among groups with or without LPS treatment and groups with different intervals between LPS treatment and *in vivo* imaging (Figure 7C and 7D). These observations indicate microglia in both acute and chronic phases after LPS treatment are able to interact with synapses with their highly dynamic processes.

Brain cytokine and chemokine profiles after LPS treatment

We next asked whether soluble factors, such as TNF-α and IL-6, in the neocortex were persistently modulated after LPS treatment. Inflammation induces the expression of a variety of cytokines and chemokines in microglia [38]. Profiles of 22 different cytokines and chemokines in lysates taken from the neocortex of mice were evaluated by using antibody array membranes. We prepared brain lysate from mice sacrificed at multiple time points (one hr, two days, or 28 days) after LPS treatment (N = 1 for one hr and two days (data not shown), N = 3 for 28 days) and from control mice (N = 3). Signals were detected by a chemiluminescence method and were compared with the signal intensity of control mice (Figure 8A and 8B). We did not detect more than a two-fold increase or decrease in the level of cytokines/chemokines tested at any time point (Figure 8C). To test the sensitivity of our membrane array system, we challenged the mice with a ten-fold higher dose of LPS (5 mg/kg) (N = 1) that reportedly induces the amoeboid transformation of microglia and up-regulation of cytokines. In this condition, we successfully detected the up regulation of some cytokines (IL-6, IL-12, and TNF-α; data not shown) as reported previously [37]. This demonstrated that the detection system was indeed capable of measuring marked changes in cytokines/chemokines. Thus, at the LPS dose used in our imaging experiments, spine turnover rate might be modulated by other soluble factors secreted from microglia. However, we can not exclude the possibility that activated microglia, which corresponds to a small fraction of the cells present in the neocortex, secreted factors whose amount is under the limit of sensitivity of our detection system.

Discussion

In this study, we addressed the question of how peripheral immune responses can modulate network remodeling of the neocortex *in vivo*. We imaged dendritic spines *in vivo* and analyzed spine dynamics over a period of several days to weeks after transient activation of the peripheral immune system with LPS. Within a week after LPS treatment, spine dynamics were low and comparable to those in control mice, indicating a minimal acute effect of systemic LPS treatment. Surprisingly, the fraction of newly formed or eliminated spines accumulated during four weeks after LPS treatment was twice as large as the proportion in control mice. The enhanced spine turnover was associated with persistent activation of microglial cells. The persistent modification of both spine dynamics and microglial activity suggests long-lasting effects of a single transient peripheral immune response on brain functions.

Peripheral immune response triggers sustained up-regulation of spine turnover *in vivo*

In vivo imaging of dendritic spines can be achieved by two different surgical techniques. The first approach, using chronic open-skull glass windows, provides clear imaging windows for efficient two-photon excitation in the deeper cortical layers without a limit on imaging time points [31]. The second approach, using thinned skull windows, gives less efficient excitation of the deep cortical layers and is limited in the number of repetitive imaging, due to the technical difficulty of thinning the same cranial tissue multiple times [22]. Previous reports indicate that the open-skull window is associated with transient glial activation, which is not present after proper thinned-skull surgery [32]. Because our research goal was to assess the influence of mild peripheral immune response on the remodeling of the neural network, we had to exclude any possibility of inducing inflammation in the brain parenchyma due to the imaging protocol itself. Therefore, we imaged dendritic spines through a thinned-skull window in this study and successfully confirmed the remarkably stable nature of dendritic spines (turnover of < 10% over one month) [22].

In order to activate the peripheral immune system, we administered a single low dose of LPS intraperitoneally. This treatment induced persistent enhancement of spine turnover in vivo. We used the lowest possible dose of LPS (0.5 mg/kg) to induce up-regulation of Iba-1 immunoreactivity in microglia and there was no sign of acute neuronal degeneration in the brain (data not shown). A previous study by Sparkman *et al.* using a single intraperitoneal injection of LPS at the low dose of 0.25 mg/kg reported the presence of classic signs of sickness behavior, including decreased locomotion, hunched posture, piloerection, and anorexia [39]. Therefore we cannot eliminate the possibility that emotional and cognitive alterations acutely induced by sickness-related behavioral changes are partly responsible for alterations in spine dynamics. On later days of in vivo imaging, however, mice are fully recovered and it is less likely that the initial sickness behavior is the direct cause of the enduring enhancement of spine dynamics. Instead, we propose that persistent activation of microglia over a period of more than several weeks plays an important role in enhanced synapse remodeling.

Synapse formation and elimination are believed to be the basis for the plastic changes of neuronal circuits

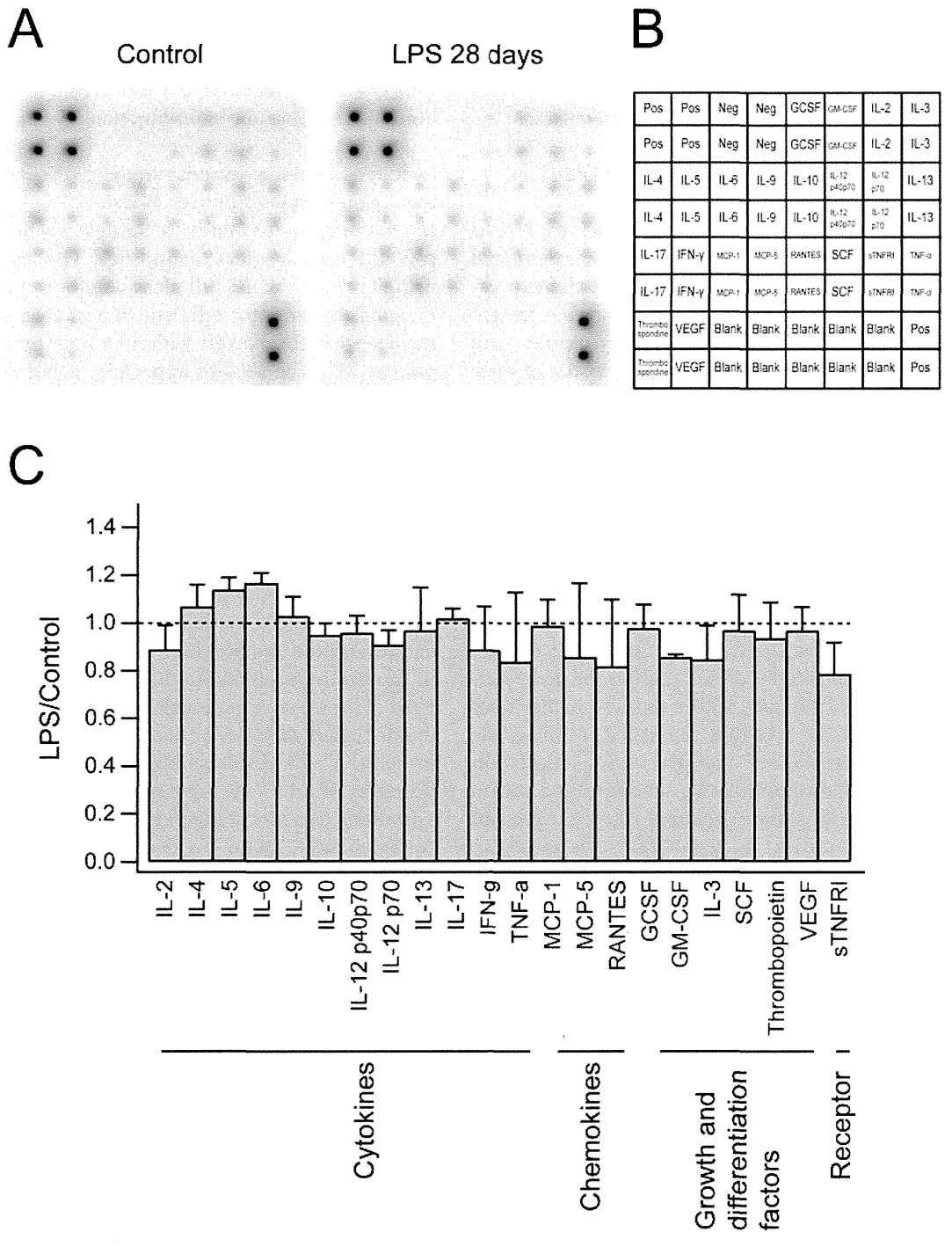

Figure 8 Brain cytokine expression after LPS treatment. (A) *Images of cytokine array membranes incubated with brain homogenates from* control mice (N = 3) and mice treated with LPS 28 days before preparation of brain homogenates (N = 3). (B) The arrangement of tested cytokines on the membrane. (C) The density of each spot was measured and the ratios between control and LPS-treated groups were calculated. There was no substantial increase or decrease in expression of the cytokines we tested.

[40,41]. Therefore changes in synaptic connections should be associated with functional changes in the neural network. Then, what are the functional outcomes of spine dynamics after LPS treatment? Interestingly, Sparkman *et al.* reported that LPS administration affected the performance of mice in the Morris water maze more profoundly on later test days [39]. The difference in distance swam became significant only after three days had elapsed following LPS injection. This time course may reflect accumulation of network remodeling in the hippocampus over the period of several days, which may be paralleled by the enhanced spine turnover we observed in the neocortex. A possible link between cognitive impairment observed in LPS-treated rodents and alterations in the neural network is reinforced by a previous study showing LPS-dependent modification of synaptic plasticity, such as LTP [9]. For example, Shaw *et al.* reported impairment of both the dentate gyrus LTP *in vivo* and performance of a water maze task in rats that received a single dose of LPS (0.25 mg/kg) intraperitoneally [42]. Cytokines up-regulated by LPS administration, such as TNFα and IL-1β, are also known to function as modulators of synaptic plasticity [43-45]. It is possible that elevation of cytokines initiated by peripheral LPS treatment modulates LTP/long-term depression (LTD)-like mechanisms *in vivo* and subsequently triggers structural remodeling of the neural network, including addition and elimination of spines.

Persistent microglial activation triggered by peripheral immune responses may be involved in enhanced spine dynamics

Neuronal networks in the mammalian forebrain are intrinsically dynamic [20,46] and are regulated by interactions with glia [19,47-49]. Microglial cells constitute the major cell type which responds to peripheral inflammation in the CNS [37]. Therefore we suspected that microglial cells directly modulated spine dynamics in response to intraperitoneal administration of LPS. As we already discussed, *in vivo* imaging through an open-skull glass window results in relatively high turnover rate of spines, together with transient activation of microglia. In contrast, with the thinned-skull window technique, much less spine dynamics and microglia activation were observed [32]. In pathological states, microglial processes show enhanced motility [17,18] and preferentially associate with synapses and may facilitate their deconstruction [19]. How microglia regulate neural networks *in vivo* is still poorly understood. Microglia may induce synapse remodeling via direct mechanical contact of their processes with synapses, or they may release soluble factors which destabilize nearby synapses. In order to evaluate these possibilities, we performed morphological and biochemical analyses of microglia in the neocortex after LPS administration.

In order to address the structural interactions between microglia and spines, we first analyzed the morphological transition of microglia with enhanced Iba1 expression after LPS administration. Iba1 is a small EF hand calcium binding protein involved in Rac and calcium signaling pathways [15]. Therefore, morphological changes of microglia could be related to the reorganization of the actin network through the Rac pathway. We observed both enhanced Iba1 expression and shrinkage of microglial processes two days after LPS treatment. This observation confirms that a single peripheral injection of LPS is sufficient to trigger activation of microglia. Iba1 expression was up-regulated between seven and 28 days after LPS administration and the number of microglia was also increased during the same period. These observations are consistent with the idea that microglia activation is not only maintained, but gradually enhanced over a time period of several weeks after LPS treatment. Our *in vivo* imaging of *Iba1-GFP* mice revealed that microglial processes had comparable motility before and after LPS treatment. Because the density of microglia increased late after LPS treatment, the frequency of individual synapses to receive contact of activated microglia may also be enhanced. This effect possibly underlies the progressive elimination of spines after LPS treatment. In the current studies, we restricted our analysis of microglial changes up to one month and we did not investigate the direct association between dendritic spines and microglial processes. However, the dynamic nature of microglial processes and their interaction with synapses were reported recently (17-19). Our present observation of the alterations in spine remodeling suggests an association with the change in microglia. Further studies are necessary to elucidate whether microglial contact is involved in the spine elimination.

Cytokines that are secreted from glial cells in the brain can affect both synaptic functions and spine morphology [43,44,50]. In animal models of neurodegenerative disorders and aging, there are reports of proliferating activated microglia and the increased levels of proinflammatory and anti-inflammatory cytokines together with impairments of spine density and morphology [51]. Systemic administration of LPS also increases several types of cytokines in the peripheral blood, mainly TNF-α, IL-1β, and IL-6 [7]. In order to detect soluble factors up-regulated in the brain during the persistent enhancement of spine turnover, we measured the levels of cytokines and chemokines in brain extracts prepared 28 days after LPS treatment. However, we were unable to detect increased expression of multiple cytokines. These results suggest that either signals

mediated by soluble factors may not be involved in synapse destabilization or, alternatively, factors we have not yet tested play a critical role. It is also possible that cytokines or chemokines we tested are indeed involved in synapse remodeling, but the concentration sufficient for exerting their effect is below the limit of detection.

In this study, we found that mild and transient peripheral inflammation induced long-lasting changes of spine dynamics over a period of several weeks and persistent up-regulation of Iba1 expression in microglia. Although we could not demonstrate convincing evidence for the interrelationship between these two alterations, recent findings showing the interaction between microglia and synapses (17-19) indicate that activation of microglia may be associated with spine remodeling. However, the relationship between microglia and spine changes in our present study remains to be fully elucidated in future experiments. The parallel sustained alterations of both spine turnover and the state of microglia in vivo may underlie long-term cognitive impairment after peripheral inflammation, which may be relevant to the neurological problems of patients who have recovered from septic conditions.

Conclusions

In this study, we used *in vivo* two-photon imaging in mice to test whether peripheral immune responses affected cortical synapses. We observed parallel increases in spine dynamics and microglial activities after LPS treatment. Although a more definitive causal relationship between spine and microglial changes should be clarified in the future, our results implicate that microglial activities may affect spine dynamics. These observations could help our understanding of the long-term cognitive impairment of septic human patients.

List of abbreviations used

GFAP: glial fibrillary acidic protein; GFP: green fluorescence protein; Iba: ionized calcium binding adaptor molecule; IL: interleukin; LPS: lipopolysaccharide; LTD: long-term depression; LTP: long-term potentiation; TNF: tumor necrosis factor.

Acknowledgements

We thank Joshua R. Sanes for the *Thy1-GFP* M mouse, together with Ryuichi Shigemoto and Haruo Kasai for transfer of available animals. We thank Wen-Biao Gan and Feng Pan for teaching surgical methods. We thank Aya Ito-Ishida for comments on the manuscript and Ayako Hayashi for help in image analysis. This work was supported by Grants-in-Aid for Scientific Research (18200025, 20019013, 21220008, and 22650070 to S.O.) from the Ministry of Education, Culture, Sports, Science and Technology of Japan and in part by Global COE Program (Integrative Life Science Based on the Study of Biosignaling Mechanisms), MEXT, Japan. A part of this study is the result of "Development of biomarker candidates for social behavior" carried out under the Strategic Research Program for Brain Sciences by the Ministry of Education, Culture, Sports, Science and Technology of Japan (S. O.), and also by Takeda Science Foundation (S. O.).

Author details

[1]Department of Cellular Neurobiology, Graduate School of Medicine, University of Tokyo, Bunkyo-ku, Tokyo 113-0033, Japan. [2]Department of Neurochemistry, National Institute of Neuroscience, Kodaira, Tokyo 187-8502, Japan.

Authors' contributions

SatK conducted experiments, analyzed data, and wrote the manuscript. ShiK generated the *Iba1-GFP* transgenic mouse. SO designed experiments, and wrote the manuscript. All authors read and approved the final manuscript.

Competing interests

The authors declare that they have no competing interests.

Received: 27 April 2011 Accepted: 17 June 2011
Published: 17 June 2011

References

1. Streck EL, Comim CM, Barichello T, Quevedo J: **The septic brain.** *Neurochem Res* 2008, **33**:2171-2177.
2. Luheshi GN: **Cytokines and fever. Mechanisms and sites of action.** *Ann N Y Acad Sci* 1998, **856**:83-89.
3. Dinarello CA: **Cytokines as endogenous pyrogens.** *J Infect Dis* 1999, **179(Suppl 2)**:S294-304.
4. Cao C, Matsumura K, Yamagata K, Watanabe Y: **Involvement of cyclooxygenase-2 in LPS-induced fever and regulation of its mRNA by LPS in the rat brain.** *Am J Physiol* 1997, **272**:R1712-1725.
5. Matsumura K, Kaihatsu S, Imai H, Terao A, Shiraki T, Kobayashi S: **Cyclooxygenase in the vagal afferents: is it involved in the brain prostaglandin response evoked by lipopolysaccharide?** *Auton Neurosci* 2000, **85**:88-92.
6. Yamagata K, Matsumura K, Inoue W, Shiraki T, Suzuki K, Yasuda S, Sugiura H, Cao C, Watanabe Y, Kobayashi S: **Coexpression of microsomal-type prostaglandin E synthase with cyclooxygenase-2 in brain endothelial cells of rats during endotoxin-induced fever.** *J Neurosci* 2001, **21**:2669-2677.
7. Dantzer R, O'Connor JC, Freund GG, Johnson RW, Kelley KW: **From inflammation to sickness and depression: when the immune system subjugates the brain.** *Nat Rev Neurosci* 2008, **9**:46-56.
8. Shaw KN, Commins S, O'Mara SM: **Lipopolysaccharide causes deficits in spatial learning in the watermaze but not in BDNF expression in the rat dentate gyrus.** *Behav Brain Res* 2001, **124**:47-54.
9. Cunningham AJ, Murray CA, O'Neill LA, Lynch MA, O'Connor JJ: **Interleukin-1 beta (IL-1 beta) and tumour necrosis factor (TNF) inhibit long-term potentiation in the rat dentate gyrus *in vitro*.** *Neurosci Lett* 1996, **203**:17-20.
10. Commins S, O'Neill LA, O'Mara SM: **The effects of the bacterial endotoxin lipopolysaccharide on synaptic transmission and plasticity in the CA1-subiculum pathway *in vivo*.** *Neuroscience* 2001, **102**:273-280.
11. Giaume C, Kirchhoff F, Matute C, Reichenbach A, Verkhratsky A: **Glia: the fulcrum of brain diseases.** *Cell Death Differ* 2007, **14**:1324-1335.
12. Nakajima K, Kohsaka S: **Microglia: neuroprotective and neurotrophic cells in the central nervous system.** *Curr Drug Targets Cardiovasc Haematol Disord* 2004, **4**:65-84.
13. Hanisch UK, Kettenmann H: **Microglia: active sensor and versatile effector cells in the normal and pathologic brain.** *Nat Neurosci* 2007, **10**:1387-1394.
14. Ransohoff RM, Perry VH: **Microglial physiology: unique stimuli, specialized responses.** *Annu Rev Immunol* 2009, **27**:119-145.
15. Ohsawa K, Imai Y, Kanazawa H, Sasaki Y, Kohsaka S: **Involvement of Iba1 in membrane ruffling and phagocytosis of macrophages/microglia.** *J Cell Sci* 2000, **113(Pt 17)**:3073-3084.
16. Imai Y, Kohsaka S: **Intracellular signaling in M-CSF-induced microglia activation: role of Iba1.** *Glia* 2002, **40**:164-174.
17. Davalos D, Grutzendler J, Yang G, Kim JV, Zuo Y, Jung S, Littman DR, Dustin ML, Gan WB: **ATP mediates rapid microglial response to local brain injury *in vivo*.** *Nat Neurosci* 2005, **8**:752-758.
18. Nimmerjahn A, Kirchhoff F, Helmchen F: **Resting microglial cells are highly dynamic surveillants of brain parenchyma *in vivo*.** *Science* 2005, **308**:1314-1318.

19. Wake H, Moorhouse AJ, Jinno S, Kohsaka S, Nabekura J: **Resting microglia directly monitor the functional state of synapses *in vivo* and determine the fate of ischemic terminals.** *J Neurosci* 2009, **29**:3974-3980.
20. Okabe S, Kim HD, Miwa A, Kuriu T, Okado H: **Continual remodeling of postsynaptic density and its regulation by synaptic activity.** *Nat Neurosci* 1999, **2**:804-811.
21. Marrs GS, Green SH, Dailey ME: **Rapid formation and remodeling of postsynaptic densities in developing dendrites.** *Nat Neurosci* 2001, **4**:1006-1013.
22. Grutzendler J, Kasthuri N, Gan WB: **Long-term dendritic spine stability in the adult cortex.** *Nature* 2002, **420**:812-816.
23. Trachtenberg JT, Chen BE, Knott GW, Feng G, Sanes JR, Welker E, Svoboda K: **Long-term *in vivo* imaging of experience-dependent synaptic plasticity in adult cortex.** *Nature* 2002, **420**:788-794.
24. Zhang S, Boyd J, Delaney K, Murphy TH: **Rapid reversible changes in dendritic spine structure *in vivo* gated by the degree of ischemia.** *J Neurosci* 2005, **25**:5333-5338.
25. Zhang S, Murphy TH: **Imaging the impact of cortical microcirculation on synaptic structure and sensory-evoked hemodynamic responses *in vivo*.** *PLoS Biol* 2007, **5**:e119.
26. Tsai J, Grutzendler J, Duff K, Gan WB: **Fibrillar amyloid deposition leads to local synaptic abnormalities and breakage of neuronal branches.** *Nat Neurosci* 2004, **7**:1181-1183.
27. Meyer-Luehmann M, Spires-Jones TL, Prada C, Garcia-Alloza M, de Calignon A, Rozkalne A, Koenigsknecht-Talboo J, Holtzman DM, Bacskai BJ, Hyman BT: **Rapid appearance and local toxicity of amyloid-beta plaques in a mouse model of Alzheimer's disease.** *Nature* 2008, **451**:720-724.
28. Feng G, Mellor RH, Bernstein M, Keller-Peck C, Nguyen QT, Wallace M, Nerbonne JM, Lichtman JW, Sanes JR: **Imaging neuronal subsets in transgenic mice expressing multiple spectral variants of GFP.** *Neuron* 2000, **28**:41-51.
29. Hirasawa T, Ohsawa K, Imai Y, Ondo Y, Akazawa C, Uchino S, Kohsaka S: **Visualization of microglia in living tissues using Iba1-EGFP transgenic mice.** *J Neurosci Res* 2005, **81**:357-362.
30. Yuste R, Bonhoeffer T: **Genesis of dendritic spines: insights from ultrastructural and imaging studies.** *Nat Rev Neurosci* 2004, **5**:24-34.
31. Holtmaat A, Bonhoeffer T, Chow DK, Chuckowree J, De Paola V, Hofer SB, Hubener M, Keck T, Knott G, Lee WC, Mostany R, Mrsic-Flogel TD, Nedivi E, Portera-Cailliau C, Svoboda K, Trachtenberg JT, Wilbrecht L: **Long-term, high-resolution imaging in the mouse neocortex through a chronic cranial window.** *Nat Protoc* 2009, **4**:1128-1144.
32. Xu HT, Pan F, Yang G, Gan WB: **Choice of cranial window type for *in vivo* imaging affects dendritic spine turnover in the cortex.** *Nat Neurosci* 2007, **10**:549-551.
33. Zuo Y, Lin A, Chang P, Gan WB: **Development of long-term dendritic spine stability in diverse regions of cerebral cortex.** *Neuron* 2005, **46**:181-189.
34. Yang G, Pan F, Gan WB: **Stably maintained dendritic spines are associated with lifelong memories.** *Nature* 2009, **462**:920-924.
35. Yasumatsu N, Matsuzaki M, Miyazaki T, Noguchi J, Kasai H: **Principles of long-term dynamics of dendritic spines.** *J Neurosci* 2008, **28**:13592-13608.
36. Guo LH, Schluesener HJ: **Acute but not chronic stimulation of glial cells in rat spinal cord by systemic injection of lipopolysaccharide is associated with hyperalgesia.** *Acta Neuropathol* 2006, **112**:703-713.
37. Qin L, Wu X, Block ML, Liu Y, Breese GR, Hong JS, Knapp DJ, Crews FT: **Systemic LPS causes chronic neuroinflammation and progressive neurodegeneration.** *Glia* 2007, **55**:453-462.
38. Graeber MB, Streit WJ: **Microglia: biology and pathology.** *Acta Neuropathol* 2010, **119**:89-105.
39. Sparkman NL, Kohman RA, Garcia AK, Boehm GW: **Peripheral lipopolysaccharide administration impairs two-way active avoidance conditioning in C57BL/6J mice.** *Physiol Behav* 2005, **85**:278-288.
40. Zuo Y, Yang G, Kwon E, Gan WB: **Long-term sensory deprivation prevents dendritic spine loss in primary somatosensory cortex.** *Nature* 2005, **436**:261-265.
41. Holtmaat A, Wilbrecht L, Knott GW, Welker E, Svoboda K: **Experience-dependent and cell-type-specific spine growth in the neocortex.** *Nature* 2006, **441**:979-983.
42. Shaw KN, Commins S, O'Mara SM: **Cyclooxygenase inhibition attenuates endotoxin-induced spatial learning deficits, but not an endotoxin-induced blockade of long-term potentiation.** *Brain Res* 2005, **1038**:231-237.
43. Beattie EC, Stellwagen D, Morishita W, Bresnahan JC, Ha BK, Von Zastrow M, Beattie MS, Malenka RC: **Control of synaptic strength by glial TNFalpha.** *Science* 2002, **295**:2282-2285.
44. Ikegaya Y, Delcroix I, Iwakura Y, Matsuki N, Nishiyama N: **Interleukin-1beta abrogates long-term depression of hippocampal CA1 synaptic transmission.** *Synapse* 2003, **47**:54-57.
45. Centonze D, Muzio L, Rossi S, Cavasinni F, De Chiara V, Bergami A, Musella A, D'Amelio M, Cavallucci V, Martorana A, Bergamaschi A, Cencioni MT, Diamantini A, Butti E, Comi G, Bernardi G, Cecconi F, Battistini L, Furlan R, Martino G: **Inflammation triggers synaptic alteration and degeneration in experimental autoimmune encephalomyelitis.** *J Neurosci* 2009, **29**:3442-3452.
46. Okabe S, Miwa A, Okado H: **Spine formation and correlated assembly of presynaptic and postsynaptic molecules.** *J Neurosci* 2001, **21**:6105-6114.
47. Ullian EM, Sapperstein SK, Christopherson KS, Barres BA: **Control of synapse number by glia.** *Science* 2001, **291**:657-661.
48. Murai KK, Nguyen LN, Irie F, Yamaguchi Y, Pasquale EB: **Control of hippocampal dendritic spine morphology through ephrin-A3/EphA4 signaling.** *Nat Neurosci* 2003, **6**:153-160.
49. Nishida H, Okabe S: **Direct astrocytic contacts regulate local maturation of dendritic spines.** *J Neurosci* 2007, **27**:331-340.
50. Boulanger LM: **Immune proteins in brain development and synaptic plasticity.** *Neuron* 2009, **64**:93-109.
51. Lucin KM, Wyss-Coray T: **Immune activation in brain aging and neurodegeneration: too much or too little?** *Neuron* 2009, **64**:110-122.

doi:10.1186/1756-6606-4-27
Cite this article as: Kondo *et al.*: Long-term changes of spine dynamics and microglia after transient peripheral immune response triggered by LPS *in vivo*. *Molecular Brain* 2011 **4**:27.